Atmospheric
Measurement
Techniques

Cirrus cloud optical and microphysical property retrievals from eMAS during SEAC[4]RS using bi-spectral reflectance measurements within the 1.88 μm water vapor absorption band

Kerry Meyer[1,2], Steven Platnick[2], G. Thomas Arnold[3,2], Robert E. Holz[4], Paolo Veglio[4], John Yorks[2], and Chenxi Wang[5]

[1]Goddard Earth Sciences Technology and Research (GESTAR), Universities Space Research Association, Columbia, Maryland, 21046, USA
[2]NASA Goddard Space Flight Center, Greenbelt, Maryland, 20771, USA
[3]Science Systems and Applications, Inc., Lanham, Maryland, 20706, USA
[4]Cooperative Institute for Meteorological Satellite Studies, University of Wisconsin, Madison, Wisconsin, 53706, USA
[5]Earth System Science Interdisciplinary Center, University of Maryland, College Park, Maryland, 20740, USA

Correspondence to: Kerry Meyer (kerry.meyer@nasa.gov)

Abstract. Previous bi-spectral imager retrievals of cloud optical thickness (COT) and effective particle radius (CER) based on the Nakajima and King (1990) approach, such as those of the operational MODIS cloud optical property retrieval product (MOD06), have typically paired a non-absorbing visible or near-infrared wavelength, sensitive to COT, with an absorbing shortwave or mid-wave infrared wavelength sensitive to CER. However, in practice it is only necessary to select two spectral channels that exhibit a strong contrast in cloud particle absorption. Here it is shown, using eMAS observations obtained during NASA's SEAC[4]RS field campaign, that selecting two absorbing wavelength channels within the broader 1.88 μm water vapor absorption band, namely the 1.83 and 1.93 μm channels that have sufficient differences in ice crystal single scattering albedo, can yield COT and CER retrievals for thin to moderately thick single-layer cirrus that are reasonably consistent with other solar and IR imager-based and lidar-based retrievals. A distinct advantage of this channel selection for cirrus cloud retrievals is that the below-cloud water vapor absorption minimizes the surface contribution to measured cloudy top-of-atmosphere reflectance, in particular compared to the solar window channels used in heritage retrievals such as MOD06. This reduces retrieval uncertainty resulting from errors in the surface reflectance assumption and reduces the frequency of retrieval failures for thin cirrus clouds.

1 Introduction

Reflectance measurements at spectral channels centered within the water vapor absorption bands at 1.38 and 1.88 μm have been shown to be well suited for detecting cirrus clouds (Gao et al., 1993). This is because cirrus clouds are typically located at high altitudes above the bulk of atmospheric water vapor; thus the contribution of the Earth's surface and boundary-layer clouds to top-of-atmosphere (TOA) reflectance at wavelength channels within these bands is negligible in sufficiently moist atmospheric conditions due to absorption by the atmospheric water vapor below the cirrus layer. Moreover, TOA reflectance of cirrus at 1.38 μm is sensitive to cloud optical thickness (COT), with only a small sensitivity to cloud effective particle radius (CER) due to weak ice crystal absorption (Kou et al., 1993; Yang et al., 2000). This sensitivity has been exploited using 1.38 μm reflectance measurements from the Moderate-resolution Imag-

ing Spectroradiometer (MODIS) for retrieving the COT of thin cirrus clouds (Meyer et al., 2004, 2007; Meyer and Platnick, 2010). Thin cirrus are often problematic for traditional passive imager cloud retrievals, such as the operational MODIS cloud optical and microphysical property products (MOD06) (Platnick et al., 2003, 2015). Because the non-absorbing visible (VIS), near-infrared (NIR), or short-wave infrared (SWIR) wavelength channels typically used for COT retrievals, as well as the absorbing SWIR and mid-wave infrared (MWIR) wavelength channels used for CER retrievals, are sensitive to reflection by the underlying surface, such approaches are subject to larger retrieval uncertainty and increased frequency of retrieval failures for thin cirrus cases.

Previous 1.38 μm based approaches, however, either require an a priori assumption about CER or necessitate the pairing of a second SWIR channel for simultaneous CER retrievals that can reintroduce surface sensitivity. Both cases can result in increased COT retrieval uncertainties, though it should be noted that surface sensitivity can be mitigated by pairing 1.38 μm with a channel centered at 1.88 μm (Gao et al., 2004). Here, a new approach is presented that pairs reflectance measurements at two narrow channels within the 1.88 μm water vapor absorption band to simultaneously retrieve cirrus COT and CER while minimizing the surface reflectance contribution. The retrieval has been applied to reflectance measurements from the Enhanced MODIS Airborne Simulator (eMAS) (King et al., 1996; Ellis et al., 2011). Retrieval results are shown for select case studies, as are comparisons with an eMAS-based version of MOD06, and retrievals from infrared (IR) approaches and from the Cloud Physics Lidar (CPL) (McGill et al., 2002).

2 Data

The eMAS (King et al., 1996), a line-scanning spectrometer deployed on NASA's high-altitude ER-2 research aircraft, measures radiances at 38 spectral channels in the wavelength range from 0.47 to 14.1 μm. With a maximum scan angle extending 43° to either side of nadir, eMAS observes 716 pixels across a 37 km wide ground swath at a nominal ER-2 altitude of 20 km, yielding pixel sizes on the Earth's surface of roughly 50 m at nadir. The ER-2 flew extensive science flights as part of the Studies of Emissions and Atmospheric Composition, Clouds and Climate Coupling by Regional Surveys (SEAC[4]RS) field campaign based in Houston, Texas, in August and September 2013, with a payload that included both the eMAS and CPL within the same wing superpod. Numerous cirrus cloud scenes were observed during SEAC[4]RS, from which the present case studies are selected.

As part of normal field campaign efforts, the eMAS team provides cloud masking and cloud property retrieval products based on the operational MODIS cloud mask (MOD35)

(Ackerman et al., 1998, 2008; Frey et al., 2008) and cloud top and optical property (MOD06) retrievals (Platnick et al., 2003). For SEAC[4]RS, these eMAS cloud products, referred to hereafter as MAS06, use the latest Collection 6 version of MOD06 that includes numerous algorithm updates and enhancements (Platnick et al., 2015) and also includes a cloud top retrieval from the NOAA Algorithm Working Group (AWG) PATMOS-x algorithm (based on the CLAVR-x algorithm used in Heidinger and Pavolonis, 2009). Note that for SEAC[4]RS, the AWG PATMOS-x algorithm provides the default cloud top retrievals, and the cloud thermodynamic phase used by the cloud optical property retrievals is provided by the heritage MOD06 Collection 5 algorithm (King et al., 2006).

In addition to MAS06, two research-level IR optimal estimation (OE) approaches have also been applied to eMAS for cirrus cloud retrievals. The first, referred to as FEANOR (Flexible Experimental Atmospheric Non-linear Optimal estimation Retrieval), uses the 8.5, 11, and 12 μm wavelength channels coupled with cloud top altitude prescribed from CPL and provides retrievals of COT and CER (Veglio and Holz, 2015). Note that for this investigation, FEANOR relies on mean IR radiances averaged over all co-located eMAS pixels within each CPL level-2 field of view, and the retrieval is only applied when CPL cloud top height (CTH) is above 8 km. The second approach, referred to here as OE-IR, also uses the 8.5, 11, and 12 μm channels, along with the 6.7, 7.2, 8.2, 12.6, 13.3, 13.6, and 13.9 μm channels, and provides full-swath pixel-level retrievals of COT, CER, and CTH (Wang et al., 2016a, b) at the native eMAS spatial resolution. The OE-IR retrievals are applied only when the cloud thermodynamic phase is ice, as determined by the MAS06 IR-derived cloud-phase algorithm (Baum et al., 2012). Both FEANOR and OE-IR provide estimates of retrieval uncertainty that account for a variety of radiometric, ancillary, and model error sources.

The availability during SEAC[4]RS of CPL also allows for additional evaluation of the eMAS retrievals. CPL is an elastic backscatter lidar that was first deployed in 2000 (McGill et al., 2002) and has participated in over 24 field campaigns aboard the NASA ER-2 and Global Hawk aircrafts. CPL measures backscatter at three wavelengths, namely 355, 532, and 1064 nm, as well as depolarization at the 1064 nm wavelength. These lidar measurements enable a comprehensive analysis of the radiative and optical properties of cirrus clouds through parameters such as CTH, depolarization ratio, backscatter and extinction coefficients, and COT (McGill et al., 2004; Davis et al., 2010; Yorks et al., 2011). For the present investigation, the CPL curtain is co-located with near-nadir eMAS observations such that the respective COT and CTH retrievals can be compared.

eMAS calibration

For remote sensing science applications, absolute radiometric calibration is a critical component. Calibration of the eMAS thermal IR channels is monitored in flight by viewing two onboard blackbody sources once every scan; the shortwave channels are calibrated in a laboratory setting pre- and post-deployment by observing Ames Airborne Facility (AAF) laboratory standard integrating hemispheres, with day-to-day fluctuations in the field monitored by a smaller portable hemisphere prior to each flight. In addition, because ambient flight conditions are significantly different from those at ground level, yielding potential inconsistencies between the laboratory calibration and that at flight altitude, periodic underflights of Terra and Aqua MODIS are used as flight-level calibration sources via statistical comparisons of collocated reflectance measurements and cloud property retrievals (e.g., King et al., 2010). Calibration is further characterized by post-campaign flights over vicarious calibration sites; for SEAC[4]RS, the site at Ivanpah Playa in Primm Valley, California, was used. The eMAS data used here include the latest available calibration corrections derived from rigorous analysis of the available satellite underflights and vicarious calibration, and they represent the eMAS team's best efforts at providing a SEAC[4]RS data set suitable for scientific investigations (Arnold et al., 2014).

3 Methodology

Though eMAS does not include the 1.38 μm channel, three narrow channels located within the 1.88 μm water vapor absorption band are available. Figure 1 shows the spectral response functions of these channels, labeled B14, B15, and B16, and centered approximately at 1.83, 1.88, and 1.93 μm, respectively, plotted over the surface to TOA two-way transmittance (gray line) calculated for a tropical ocean atmosphere using the Line-by-Line Radiative Transfer Model (LBLRTM) (Clough et al., 1992, 2005; Clough and Iacono, 1995), for a nadir view and overhead sun. It is evident that the 1.88 μm channel (B15) is located almost wholly within the broader absorption region, though the tails of the 1.83 and 1.93 μm channel response functions extend beyond the region of total attenuation. Surface effects are thus not completely screened at 1.83 and 1.93 μm as they are at 1.38 μm and the central 1.88 μm channel, even in moist atmospheres, though the contribution of surface reflection to TOA reflectance and retrieval uncertainty is substantially smaller than in the VIS/NIR/SWIR channels commonly used for COT and CER retrievals; moreover, contamination by low-altitude clouds is likely larger than at 1.38 or 1.88 μm. However, thresholds on the central 1.88 μm channel reflectance (must be larger than 0.02) and the 1.88/0.65 μm channel reflectance ratio (must be larger than 0.09) are used here to identify and remove clear-sky and low-altitude cloud pixels,
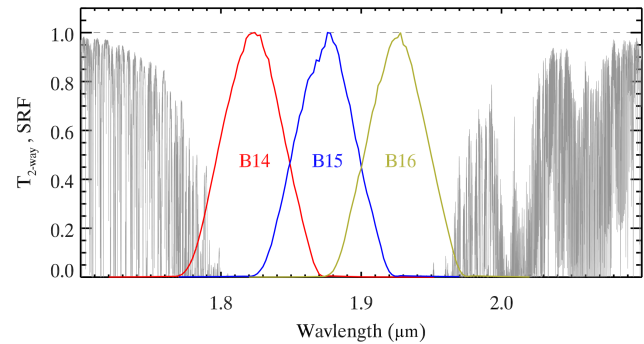

Figure 1. Spectral two-way transmittance (gray line), from TOA to surface, calculated with LBLRTM using a tropical ocean atmosphere. Spectral response functions during the SEAC4RS campaign for eMAS bands 14, 15, and 16 (band centers at approximately 1.83, 1.88, and 1.93 μm, respectively) are also shown (red, blue, and gold lines, respectively).
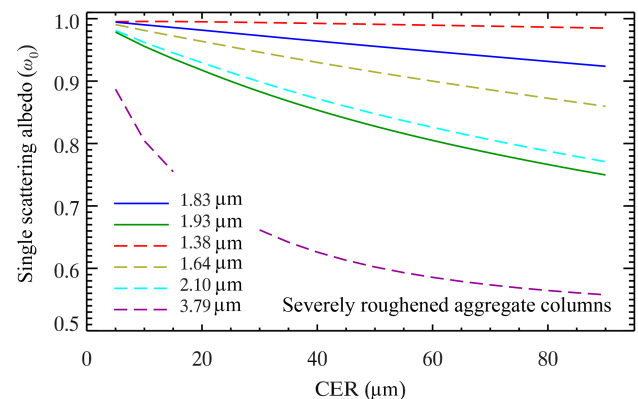

Figure 2. Bulk single scatter albedo (ω_0) for severely roughened aggregate hexagonal column ice crystals as a function of cloud effective particle radius (CER) for the eMAS 1.83 and 1.93 μm channels (blue and green, respectively) and the MODIS 1.38, 1.64, 2.1, and 3.79 μm channels (dotted red, gold, light blue, and magenta, respectively).

respectively, that may otherwise be spuriously identified as thin cirrus using only the 1.83 and 1.93 μm channels. In addition, the case studies selected here only include ocean scenes for which the surface is dark; thus the contribution of surface reflection to measured TOA cirrus reflectance is expected to be negligible.

The 1.88 μm spectral region also exhibits markedly stronger ice crystal absorption than at 1.38 μm, and TOA reflectance is consequently more sensitive to particle size. The previous techniques utilizing 1.38 μm for single-channel cirrus COT retrievals (e.g., Meyer and Platnick, 2010), which require a priori assumptions of CER, will have much larger uncertainties when applied to the channels near 1.88 μm and are thus ill suited for this spectral region. However, a strong contrast in single scattering albedo (ω_0) is evident between the 1.83 and 1.93 μm channels, indicating stronger ice crys-

tal absorption at the latter wavelength. Figure 2 shows ω_0 as a function of CER for the 1.83 μm (blue line) and 1.93 μm (green line) channels, as well as for the 1.38, 1.64, 2.1, and 3.79 μm MODIS channels (red, gold, light blue, and magenta dashed lines, respectively). The single scattering properties used here are for the severely roughened aggregate of hexagonal columns ice crystal habit (Yang et al., 2013) that was used to create the MOD06 and MAS06 ice cloud retrieval look-up tables (LUTs); note this ice crystal radiative model has been shown to provide better closure between VIS/NIR, IR, and lidar retrievals of cirrus COT (Holz et al., 2015). The contrast of ω_0 between 1.83 and 1.93 μm suggests the possibility of a bi-spectral retrieval technique for simultaneously inferring COT and CER for two absorbing channels in the manner of Nakajima and King (1990) and Platnick et al. (2001).

Figure 3 shows the bi-spectral dependence of 1.83 and 1.93 μm top-of-cloud reflectance on COT and CER when the cosines of the solar and view zenith angles are 0.9 and the relative azimuth angle is 120°. Here, spectral top-of-cloud reflectance is obtained from forward radiative transfer (RT) calculations, ignoring atmospheric gaseous absorption and assuming a black, non-reflecting surface, using the Discrete Ordinates Radiative Transfer (DISORT) algorithm (Stamnes et al., 1988). It is clear that 1.93 μm is quite sensitive to CER, and 1.83 μm is sensitive to thin to moderately thick COT, though it becomes insensitive roughly around COT = 20. In addition, because the 1.83 μm channel is also sensitive to CER, as shown by the plot of ω_0 in Fig. 2, the LUT is largely non-orthogonal. While non-orthogonal LUTs are not ideal and imply larger retrieval uncertainties, the sensitivities of the two wavelengths are such that a bi-spectral retrieval can nevertheless be performed for cirrus clouds, which are often tenuous and less optically thick.

Like the 1.38 μm channel, however, the water vapor absorption that attenuates the surface reflection at 1.83 and 1.93 μm, thus allowing sensitivity to very thin cirrus clouds, can also introduce biases in the measured cloudy sky TOA reflectances. This is because a non-negligible portion of atmospheric water vapor resides above cirrus clouds, which attenuates the measured cloudy TOA reflectances. To account for this above-cloud attenuation in both the 1.83 and 1.93 μm channels, the above-cloud water vapor profile at each eMAS pixel is found by coupling the retrieved pixel-level CTH from the AWG PATMOS-x algorithm now integrated into MAS06 with co-located ancillary atmospheric profiles obtained from the National Centers for Environmental Prediction (NCEP) Global Data Assimilation System (GDAS) 6 h "final run" archive analyses (Derber et al., 1991). The correlated k-distribution technique (e.g., Kratz, 1995; Liu et al., 2015) is used to calculate atmospheric layer spectral transmittances from the above-cloud water vapor profile that can be integrated to estimate the pixel-level above-cloud column two-way spectral transmittance from TOA to cloud top to ER-2 flight level. The above-cloud column two-way spectral trans-
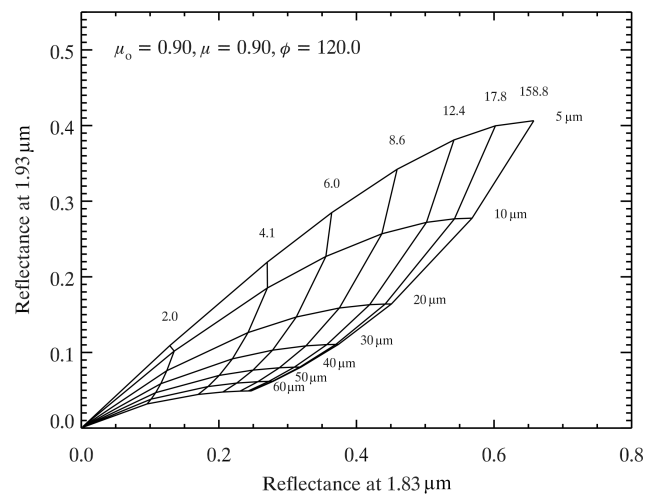

Figure 3. Two-channel plot illustrating the sensitivity of the 1.83 and 1.93 μm eMAS channels to cloud optical thickness (near-vertical lines) and effective particle radius (near-horizontal lines), respectively.

mittances are then used to calculate the respective atmospherically corrected reflectances that are in turn used to infer COT and CER from pre-computed ice cloud LUTs. The LUTs are derived under assumptions identical to MOD06/MAS06, i.e., using DISORT and the scattering properties of severely roughened aggregates of hexagonal columns (Yang et al., 2013), which are integrated over a modified gamma size distribution (effective variance 0.1) as well as the appropriate eMAS spectral response functions.

It should be noted that the present retrieval technique does not explicitly account for water vapor absorption within the cloud layer itself, which can be non-negligible for the spectral channels used here. Like MOD06/MAS06, however, the use of CTH derived from the thermal IR channels for above-cloud atmospheric absorption corrections is expected to at least partially account for the in-cloud absorption, since such radiative cloud top retrievals have been shown to be lower than the physical cloud top detected by lidar (see, e.g., Holz et al., 2008). Thus to the extent that the radiative cloud top is below the physical cloud top, the path length from TOA to the radiative cloud top is expected to include part of the cloud layer itself. Nevertheless, for the case studies shown here (see Sect. 4), the AWG PATMOS-x cloud top retrievals are near the physical cloud top detected by CPL. A sensitivity analysis (not shown) reveals that ignoring in-cloud water vapor absorption at 1.83 and 1.93 μm yields atmospherically corrected reflectance that is biased low at both channels by roughly 1–2 % for optically thick clouds and approaching a maximum low bias of 7–8 % at COT = 1; such errors correspond to low-biased COT by roughly the same magnitude at COT = 1, and CER low biases about double that magnitude. That said, in practice it is impractical to estimate the exact in-cloud water vapor absorption (or the errors resulting from

its neglect) at pixel level due in part to the lack of a computationally efficient online RT algorithm that necessitates the use of pre-computed LUTs, as well as the general ignorance of the retrieval algorithm to pixel-level radiative cloud top retrieval biases.

Retrieval uncertainty

The pixel-level retrieval solutions are found using Newtonian iteration to locate the minimum of a cost function defined in terms of the difference between the observed and forward-modeled LUT spectral reflectances; note no a priori is assumed, and thus the cost function simplifies to the weighted least squares estimate (Rodgers, 1976; Heidinger and Stephens, 2000; Cooper et al., 2003). A critical component of this approach is defining an appropriate estimate of measurement errors. The resulting measurement error covariance matrix is coupled with the forward-modeled Jacobian, or retrieval solution space sensitivity matrix (derived here from the forward-modeled retrieval LUTs), to provide a baseline retrieval uncertainty estimate that accounts for known error sources. Here, multiple error components are assumed to contribute to the total retrieval uncertainty: namely radiometric errors, atmospheric water vapor profile errors, and cloud model errors (specifically size distribution effective variance). Because the 1.83 and 1.93 μm channels are assumed to be nominally free of surface contamination in the over-ocean case studies shown here, uncertainty due to surface albedo error is not considered.

For eMAS, because ambient conditions at flight level are often not stable (a problem exacerbated by in-flight altitude changes) and can be substantially different from the laboratory conditions under which pre- and post-deployment calibration is typically performed, the absolute pixel-level radiometric uncertainty is unknown. Therefore a constant relative reflectance error, here 10 %, is assumed at both 1.83 and 1.93 μm; note that for MAS06, reflectance errors are assumed to be 5 % for 3.7 μm, 10 % for 1.6 μm, and 7 % for the remaining channels. Water vapor profile errors are assumed to be 20 % at all atmospheric layers. For cloud model uncertainty, expected reflectance errors are estimated using forward RT calculations to determine TOA reflectance deviations due to changes in the effective variance (from 0.1 to 0.05 and 0.2) of the assumed ice particle size distributions used to integrate the single scattering properties of Yang et al. (2013). Note uncertainty due to an incorrect ice crystal habit assumption, which can vary widely in nature (van Diedenhoven et al., 2014) and is expected to contribute significantly to retrieval uncertainty yet in practice is difficult to quantify, is presently ignored, as it is in both MOD06 and MAS06.

4 Results

On the 18 September 2013 SEAC[4]RS science flight, the ER-2 overflew thin to moderately thick cirrus over the Gulf of Mexico (flight track 8), as shown in the true color RGB (0.65–0.55–0.47 μm) in Fig. 4a; the direction of travel of the ER-2 in this figure is from top to bottom. AWG PATMOS-x CTH retrievals for this scene are shown in (b). The corresponding retrieved COT from MAS06 is shown in (c); note MAS06 retrievals for both ice- and liquid-phase clouds are shown and can be identified by the dual-phase color bar at top right (warm colors for liquid, cool colors for ice). COT from the 1.83 μm channel is shown in (d). Disregarding any errors in the MAS06 cloud thermodynamic phase discrimination, the 1.83 μm COT retrievals appear consistent with those from MAS06. Given the identical cloud radiative model assumptions and forward RT code used in both retrievals, this result is encouraging and bestows confidence in the above-cloud water vapor attenuation correction.

Note also the larger spatial extent of the 1.83 μm COT retrievals compared to those of MAS06. As implied by the CTH retrievals in (b), the cloud mask evidently identifies clouds throughout this scene, while the MAS06 COT retrievals imply large cloud-free regions (gray color). Disregarding potential cloud mask errors, specifically false positive cloudy pixels, the cloud-free regions indicate MAS06 COT retrieval failures, i.e., the reflectance observations are outside of the LUT retrieval solution space. The larger spatial extent of the 1.83 μm COT retrievals, however, indicates a lower occurrence of retrieval failure, an expected result of the relative insensitivity of the 1.83 and 1.93 μm channels to surface reflection, particularly for the case of optically thin cirrus clouds. In addition, the RGB image implies the presence of low-altitude liquid-phase clouds underlying the cirrus layer. These clouds are also evident in the MAS06 COT image (c) as the liquid-phase retrievals in the cirrus-free portions of the track, as well as the relatively large (i.e., bright green) COT features within the optically thinner portions of the cirrus. Note, however, that these COT features within the thin cirrus are not evident in the 1.83 μm COT image, implying potential multilayer cloud detection capabilities of reflectance measurements within the 1.88 μm water vapor band.

Conversely, CER, shown in Fig. 4e–h, exhibits less agreement in terms of retrieval magnitude, though the spatial CER patterns appear consistent. Here, CER retrievals are shown for the standard MAS06 CER channels, namely (e) 1.6 μm, (f) 2.1 μm, and (g) 3.7 μm, as well as for the 1.93 μm channel (h). Again, both liquid- and ice-phase MAS06 retrievals are shown and can be identified by the dual-phase color bar at bottom right. Disagreement between CER retrievals is not unexpected, in part because photon penetration depth within clouds has been shown to be spectrally dependent in the SWIR and MWIR (Platnick, 2000), though it is interesting to note that the 1.93 μm CER appears to have better agree-
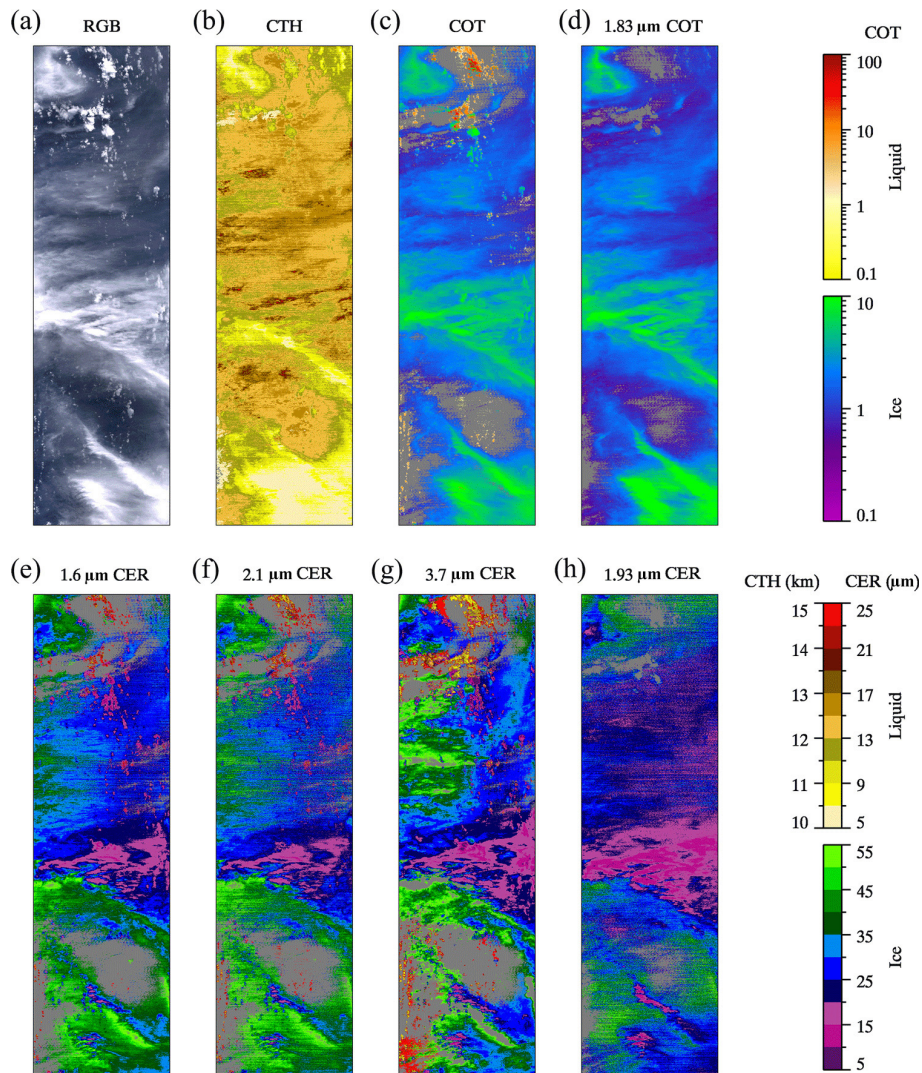
Figure 4. eMAS CTH, COT, and CER retrievals for a portion of track 8 of the 18 September 2013 SEAC[4]RS science flight. The direction of travel of the ER-2 is from top to bottom in each panel. **(a)** True color RGB (0.65–0.55–0.47 µm).

ment with the 3.7 µm CER. Similar to the COT retrievals, the presence of underlying low-altitude liquid-phase clouds is evident in the MAS06 CER retrievals by the relatively small (purple) features within the optically thin portions of the cirrus, while these features are not evident in the 1.93 µm retrievals.

A comparison of nadir-view COT, CER, and CTH retrievals for the 13 September 2013 flight track of Fig. 4 is shown in Fig. 5; the earliest-time retrievals (left) correspond to the top of each panel in Fig. 4. Plotted in (a) are eMAS-based COT retrievals from MAS06 (red), the 1.83/1.93 µm channel pair (blue), the FEANOR IR optimal estimation technique (magenta), and the multi-channel OE-IR technique (gold) (Wang et al., 2016a, b), as well as collocated 532 nm COT retrievals from CPL (green) (McGill et al., 2002); CER retrievals from MAS06 2.1 µm, FEANOR, OE-IR, and

1.83/1.93 µm are plotted in (b). To assess the CTH assumption used for above-cloud water vapor attenuation correction, the MAS06 (AWG PATMOS-x) CTH retrievals are plotted in (c) along with those from CPL and OE-IR. The vertical bars for the eMAS-based retrievals in each panel denote $\pm 1\sigma$ retrieval uncertainty. Each MAS06, OE-IR, and 1.83/1.93 µm point in this plot represents the mean retrieval over all eMAS pixels having successful retrievals within the collocated CPL product footprint, and the respective retrieval fractions within each CPL footprint must be larger than 0.25 for inclusion here; as stated above, the FEANOR retrievals use the mean spectral IR radiances averaged over all eMAS pixels within the collocated CPL footprint. Note that the MAS06 retrievals are filtered by the optical property phase product such that only the ice-phase pixels shown in Fig. 4c and e–g contribute to the means and cloud retrieval fractions, while the
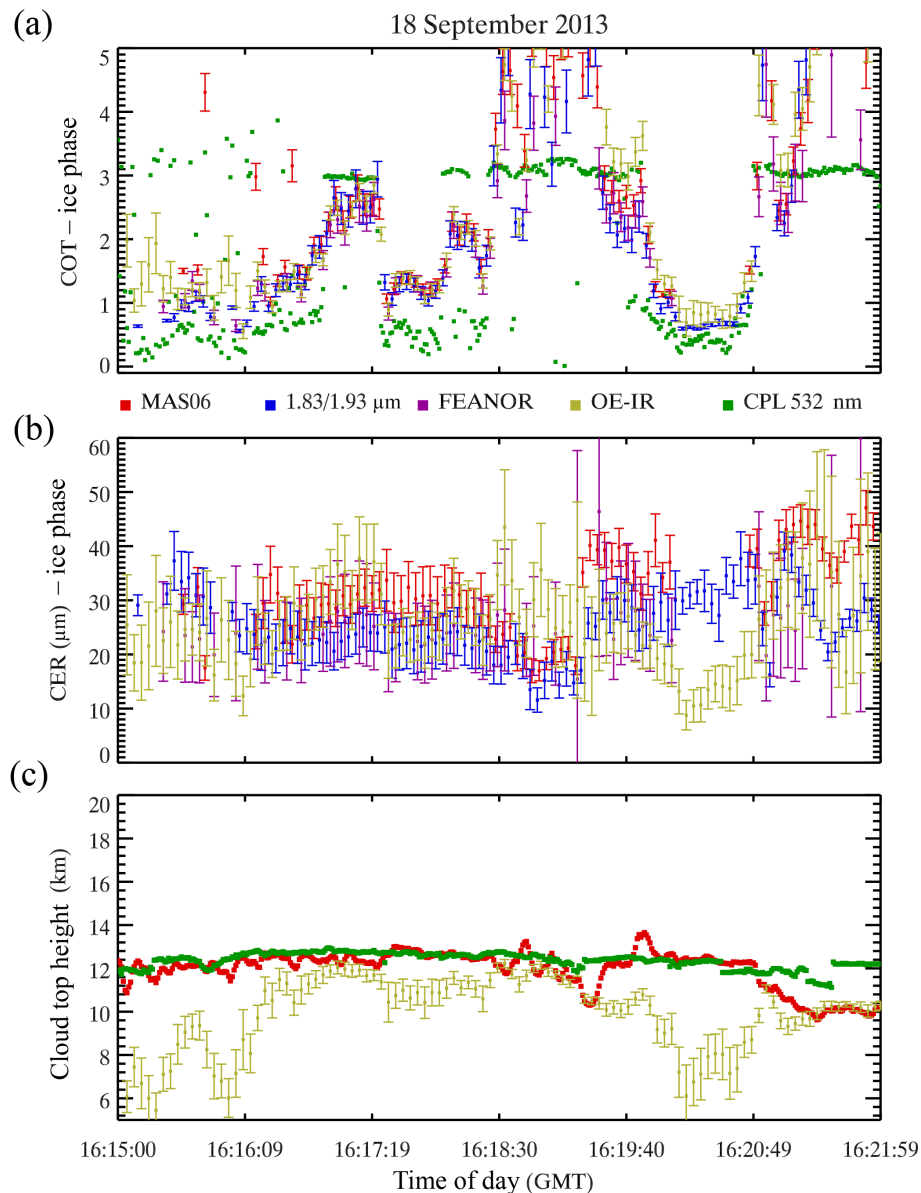
Figure 5. A comparison of nadir-view ice-phase COT **(a)**, CER **(b)**, and CTH **(c)** retrievals for the same track as in Fig. 6; the earliest-time retrievals correspond to the top of each panel in Fig. 6. Vertical bars indicate estimated retrieval uncertainties. The retrievals plotted here are from MAS06 (red), the 1.83/1.93 µm approach (blue), FEANOR optimal estimation (magenta), and OE-IR (gold), as well as collocated CPL 532 nm (green); note the MAS06 CER retrievals are those using the 2.1 µm channel.

1.83/1.93 µm retrieval means and fractions are not filtered by MAS06 phase and include all cloudy pixels having successful retrievals; the OE-IR retrievals are filtered by the MAS06 IR-derived phase product. There is overall good agreement between all COT retrievals, in particular those from eMAS, and the CER retrievals, while divergent in some regions, nonetheless exhibit some overlap when considering the retrieval uncertainties.

Figure 6 shows the full-swath eMAS retrievals for a later ER-2 segment (flight track 10) of the same 18 September

2013 SEAC^{4}RS science flight; the direction of travel of the ER-2 in this figure is again from top to bottom. Similar to Fig. 4, thin to moderately thick cirrus overlies the Gulf of Mexico, with scattered low-altitude liquid-phase clouds evident in some portions of the RGB image, as well as the MAS06 COT and CER retrieval images. Figure 7 shows the nadir-view COT, CER, and CTH retrievals for this track. As in Figs. 4 and 5, the COT retrievals all exhibit general agreement in magnitude and spatial patterns, while the CER retrievals exhibit less agreement, though the MAS06 and
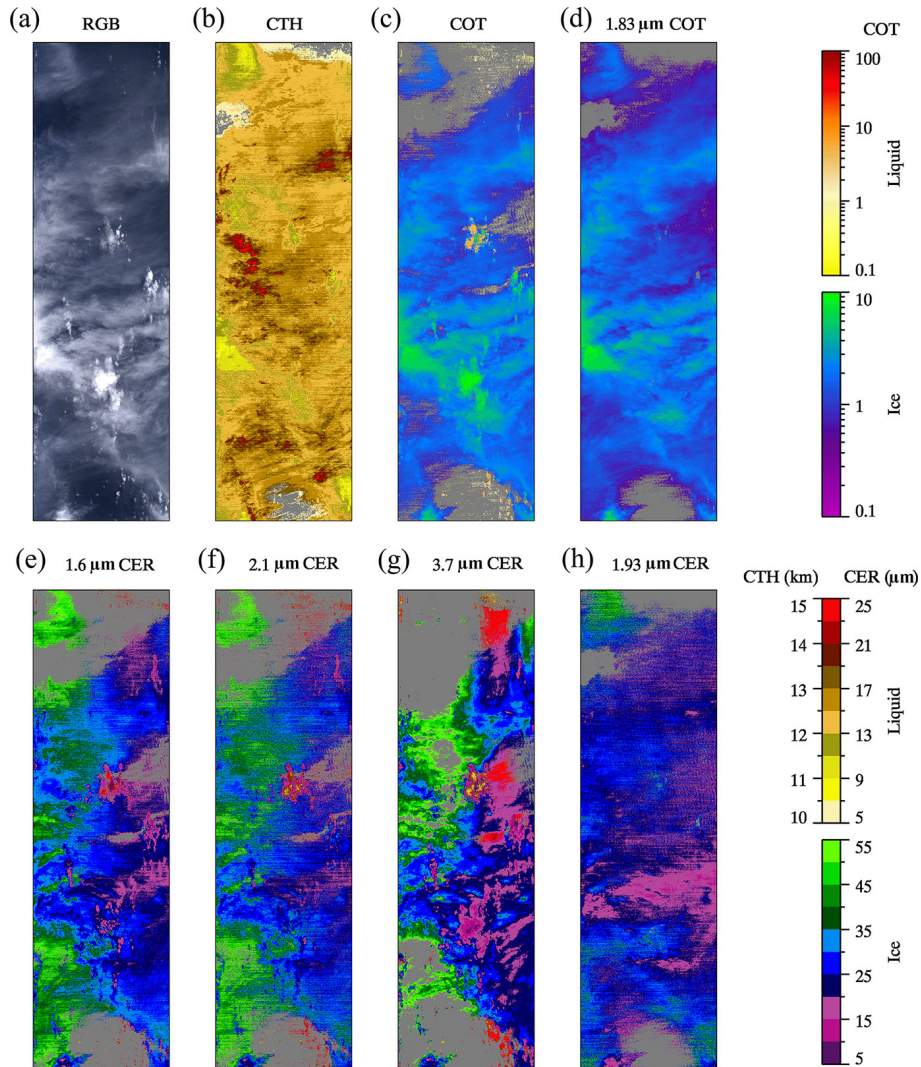
Figure 6. Same as Fig. 4 but for a portion of track 10 of the 18 September 2013 SEAC[4]RS science flight. The direction of travel of the ER-2 is again from top to bottom in each panel.

1.93 μm CER retrievals have similar spatial patterns in both the full-swath and nadir-view plots. In addition, the larger spatial extent of the 1.83/1.93 μm retrievals is evident in both figures, again indicating less frequent retrieval failures using this channel pair.

5 Discussion

Previous bi-spectral imager retrievals of COT and CER based on the Nakajima and King (1990) approach, such as those of the operational MODIS cloud optical property product (MOD06), have typically paired a non-absorbing VIS or NIR wavelength channel, sensitive to COT, with an absorbing SWIR or MWIR wavelength channel sensitive to CER. However, TOA reflectance measurements in these spectral channels can be quite sensitive to contributions from surface reflection, in particular for the case of optically thin cirrus clouds. Thus cirrus retrieval approaches that rely on these channels are often subject to larger retrieval uncertainty and increased retrieval failure frequency (i.e., reflectance observations that are outside the retrieval solution space) since they require appropriate assumptions regarding spectral surface reflection.

In practice it is only necessary to select two spectral channels that exhibit a strong contrast in cloud particle absorption. Here it is shown that two absorbing wavelength channels within the broader 1.88 μm water vapor absorption band, namely the 1.83 and 1.93 μm channels, have sufficient differences in ice crystal single scattering albedo such that a bi-spectral COT–CER retrieval approach can be applied. A distinct advantage of this channel selection for cirrus cloud retrievals is that the surface contribution to measured cloudy TOA reflectance in these channels is minimized
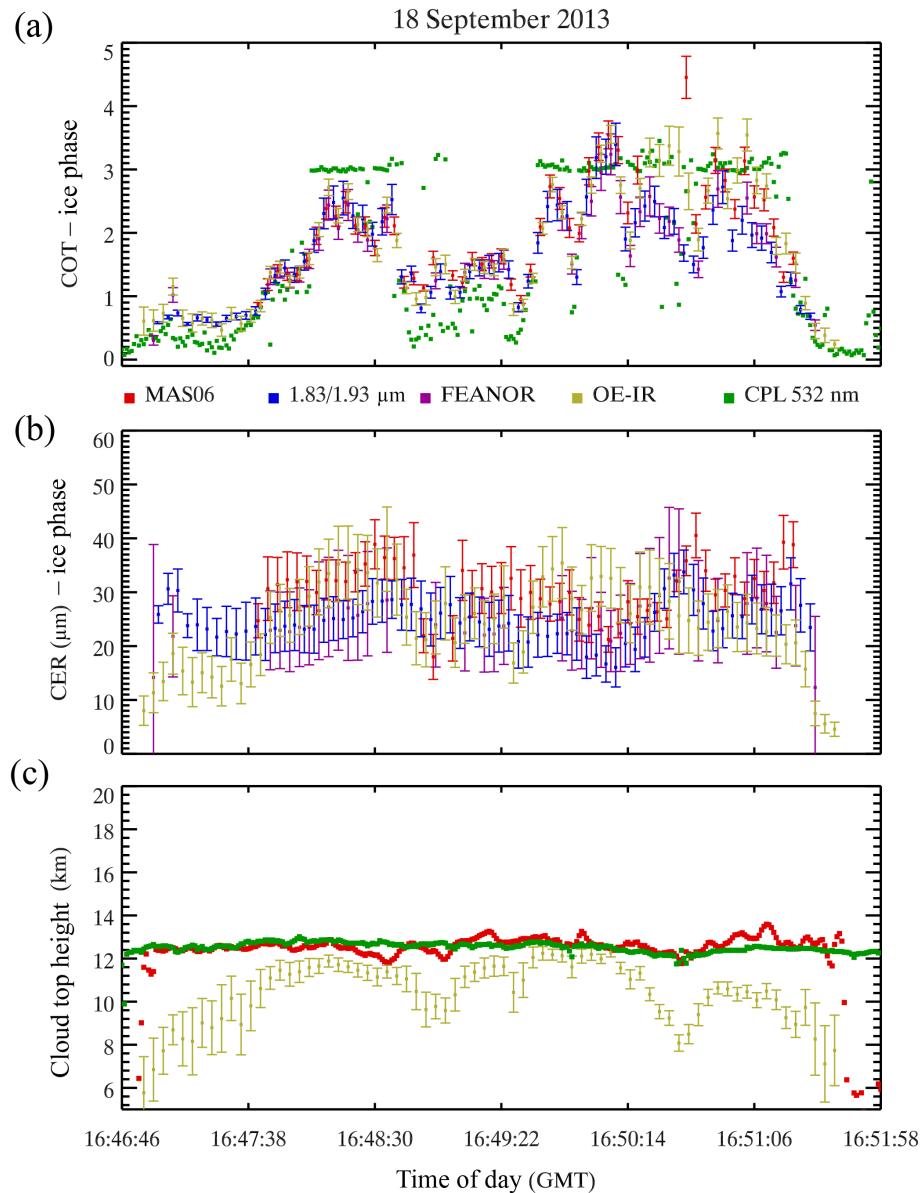
Figure 7. Same as Fig. 5 but for the track shown in Fig. 6.

due to below-cloud water vapor absorption, thus reducing retrieval uncertainty due to errors in the surface reflection assumption as well as reducing the occurrence of retrieval failures. Using two cirrus cloud case studies observed by eMAS over the Gulf of Mexico during NASA's SEAC^{4}RS field campaign, it is shown that the 1.83/1.93 μm channel pair can yield COT and CER retrievals for thin to moderately thick single-layer cirrus that are reasonably consistent with other solar and IR imager-based retrievals, as well as lidar-based COT retrievals from collocated CPL. It is also shown that the present approach can provide useful information in multilayer cloud cases, i.e., cirrus overlying low-altitude liquid clouds, again due to the below-cirrus water vapor absorption

that results in the reduced sensitivity of TOA reflectance at 1.83 and 1.93 μm to low-altitude clouds.

Finally, it is worth reemphasizing that, unlike the 1.38 and central 1.88 μm wavelength channels, below-cirrus atmospheric water vapor absorption does not completely attenuate the contribution of surface reflection in the 1.83 and 1.93 μm channels (see Fig. 1). Nevertheless, the surface contribution is substantially smaller than that in the VIS/NIR/SWIR window channels commonly used for COT and CER retrievals. For the case studies shown here, scenes over dark ocean were intentionally selected such that the contribution of surface reflection to the measured TOA reflectance at 1.83 and 1.93 μm is negligible. A more general application of the present tech-

nique over all surface types requires reasonable assumptions for surface reflection at 1.83 and 1.93 µm, even though the surface contribution nonetheless is greatly minimized. Such efforts, however, are left for future investigations.

Data availability

The eMAS level-1 data used in this investigation are publicly available and were obtained from the NASA Level 1 and Atmosphere Archive and Distribution System (LAADS) (http://ladsweb.nascom.nasa.gov); the CPL data are courtesy of the CPL science team (Matt McGill and co-author John Yorks).

References

Ackerman, S. A., Strabala, K. I., Menzel, W. P., Frey, R. A., Moeller, C. C., and Gumley, L. E.: Discriminating clear-sky from clouds with MODIS, J. Geophys. Res., 103, 32141–32157, 1998.

Ackerman, S. A., Holz, R. E., Frey, R., Eloranta, E. W., Maddux, B. C., and McGill, M.: Cloud detection with MODIS. Part II: Validation, J. Atmos. Ocean. Tech., 25, 1073–1086, doi:10.1175/2007JTECHA1053.1, 2008.

Arnold, G. T., Dominguez, R., Platnick, S., Myers, J., and Meyer, K.: eMAS solar reflectance band calibration for SEAC4RS, available at: http://mas.arc.nasa.gov/data/configs/eMAS_Solar_Reflectance_Band_Calibration_for_SEAC4RS.pdf, 2014.

Baum, B. A., Menzel, W. P., Frey, R. A., Tobin, D. C., Holz, R. E., Ackerman, S. A., Heidinger, A. K., and Yang, P.: MODIS cloud-top property refinements for Collection 6, J. Appl. Meteorol. Clim., 51, 1145–1163, doi:10.1175/JAMC-D-11-0203.1, 2012.

Clough, S. A., Iacono, M. J., and Moncet, J.-L.: Line-by-line calculation of atmospheric fluxes and cooling rates: Application to water vapor, J. Geophys. Res., 97, 15761–15785, 1992.

Clough, S. A., Shephard, M. W., Mlawer, E. J., Delamere, J. S., Iacono, M. J., Cady-Pereira, K., Boukabara, S., and Brown, P. D.: Atmospheric radiative transfer modeling: A summary of the AER codes, J. Quant. Spectrosc. Ra., 91, 233–244, 2005.

Clough, S. A. and Iacono, M. J.: Line-by-line calculations of atmospheric fluxes and cooling rates II: Application to carbon dioxide, ozone, methane, nitrous oxide, and the halocarbons, J. Geophys. Res., 100, 16519–16535, 1995.

Cooper, S. J., L'Ecuyer, T. S., and Stephens, G. L.: The impact of explicit cloud boundary information on ice cloud microphysical property retrievals from infrared radiances, J. Geophys. Res., 108, 4107, doi:10.1029/2002JD002611, 2003.

Davis, S., Hlavka, D., Jensen, E., Rosenlof, K., Yang, Q., Schmidt, S., Borrmann, S., Frey, W., Lawson, P., Voemel, H., and Bui, T. P.: In situ and lidar observations of tropopause subvisible cirrus clouds during TC4, J. Geophys. Res., 115, D00J17, doi:10.1029/2009JD013093, 2010.

Derber, J. C., Parrish, D. F., and Lord, S. J.: The new global operational analysis system at the National Meteorological Center, Weather Forecast., 6, 538–547, 1991.

Ellis, T. A., Myers, J., Grant, P., Platnick, S., Guerin, D. C., Fisher, J., Song, K., Kimchi, J., Kilmer, L., LaPorte, D. D., and Moeller, C. C.: The NASA enhanced MODIS airborne simulator, Proc. SPIE 8153, Earth Observing Systems XVI, 81530N (13 September 2011), doi:10.1117/12.894482, 2011.

Frey, R. A., Ackerman, S. A., Liu, Y., Strabala, K. I., Zhang, H., Key, J. R., and Wang, X.: Cloud detection with MODIS. Part I: Improvements in the MODIS cloud mask for Collection 5, J. Atmos. Ocean. Tech., 25, 1057–1072, doi:10.1175/2008JTECHA1052.1, 2008.

Gao, B.-C., Goetz, A. F. H., and Wiscombe, W. J.: Cirrus cloud detection from airborne imaging spectrometer data using the 1.38 µm water vapor band, Geophys. Res. Lett., 20, 301–304, doi:10.1029/93GL00106, 1993.

Gao, B.-C., Meyer, K., and Yang, P.: A new concept on remote sensing of cirrus optical depth and effective ice particle size using strong water vapor absorption channels near 1.38 and 1.88 µm, IEEE T. Geosci. Remote, 42, 1891–1899, doi:10.1109/TGRS.2004.833778, 2004.

Heidinger, A. K. and Pavolonis, M. J.: Gazing at cirrus clouds for 25 years through a split window, part I: Methodology, J. Appl. Meteorol. Clim., 48, 1100–1116, 2009.

Heidinger, A. K. and Stephens, G. L.: Molecular line absorption in a scattering atmosphere. Part II: Application to remote sensing in the O_2 A band, J. Atmos. Sci., 57, 1615–1634, 2000.

Holz, R. E., Ackerman, S. A., Nagle, F. W., Frey, R., Dutcher, S., Kuehn, R. E., Vaughan, M. A., and Baum, B.: Global Moderate Resolution Imaging Spectroradiometer (MODIS) cloud detection and height evaluation using CALIOP, J. Geophys. Res., 113, D00A19, doi:10.1029/2008JD009837, 2008.

Holz, R. E., Platnick, S., Meyer, K., Vaughan, M., Heidinger, A., Yang, P., Wind, G., Dutcher, S., Ackerman, S., Amarasinghe, N., Nagle, F., and Wang, C.: Resolving ice cloud optical thickness biases between CALIOP and MODIS using infrared retrievals, Atmos. Chem. Phys. Discuss., 15, 29455–29495, doi:10.5194/acpd-15-29455-2015, 2015.

King, M., Platnick, S., Hubanks, P. A., Arnold, G. T., Moody, E. G., Wind, G., and Wind, B.: Collection 005 Change Summary for the MODIS Cloud Optical Properties (06-OD) Algorithm, NASA, available at: http://modis-atmos.gsfc.nasa.gov/_docs/C005CloudOpticalPropertiesver3.3.pdf, 2006.

King, M. D., Menzel, W. P., Grant, P. S., Myers, J. S., Arnold, G. T., Platnick, S. E., Gumley, L. E., Tsay, S.-C., Moeller, C. C., Fitzgerald, M., Brown, K. S., and Osterwisch, F. G.: Airborne scanning spectrometer for remote sensing of cloud, aerosol, wa-

ter vapor, and surface properties, J. Atmos. Ocean. Tech., 13, 777–794, 1996.

King, M. D., Platnick, S., Wind, G., Arnold, G. T., and Dominguez, R. T.: Remote sensing of radiative and microphysical properties of clouds during TC4: Results from MAS, MASTER, MODIS, and MISR, J. Geophys. Res., 115, D00J07, doi:10.1029/2009JD013277, 2010.

Kou, L., Labrie, D., and Chylek, P.: Refractive indices of water and ice in the 0.65- to 2.5 μm spectral range, Appl. Optics, 32, 3531–3540, doi:10.1364/AO.32.003531, 1993.

Kratz, D. P.: The correlated k-distribution technique as applied to the AVHRR channels, J. Quant. Spectrosc. Ra., 53, 501–517, 1995.

McGill, M., Hlavka, D., Hart, W., Scott, V. S., Spinhirne, J., and Schmid, V.: Cloud Physics Lidar: instrument description and initial measurement results, Appl. Optics, 41, 3725–3734, 2002.

McGill, M. J., Li, L., Hart, W. D., Heymsfield, G. M., Hlavka, D. L., Racette, P. E., Tian, L., Vaughan, M. A., and Winker, D. M.: Combined lidar-radar remote sensing: initial results from CRYSTAL-FACE, J. Geophys. Res., 109, D07203, doi:10.1029/2003JD004030, 2004.

Meyer, K. and Platnick, S.: Utilizing the MODIS 1.38 μm channel for cirrus cloud optical thickness retrievals: Algorithm and retrieval uncertainties, J. Geophys. Res., 115, D24209, doi:10.1029/2010JD014872, 2010.

Meyer, K., Yang, P., and Gao, B.-C.: Optical thickness of tropical cirrus clouds derived from the MODIS 0.66- and 1.375- μm channels, IEEE T. Geosci. Remote, 42, 833–841, doi:10.1109/TGRS.2003.818939, 2004.

Meyer, K., Yang, P., and Gao, B.-C.: Ice cloud optical depth from MODIS cirrus reflectance, IEEE Geosci. Remote S., 4, 471–474, doi:10.1109/LGRS.2007.897428, 2007.

Nakajima, T. and King, M. D.: Determination of the optical thickness and effective particle radius of clouds from reflected solar radiation measurements part I: Theory, J. Atmos. Sci., 47, 1878–1893, 1990.

NASA: Enhanced MODIS Airborne Simulator (eMAS) level-1 radiometric and geolocation products, Dataset, ftp://ladsweb.nascom.nasa.gov/MAS_eMAS/, 2015a.

NASA: Enhanced MODIS Airborne Simulator (eMAS) level-2 cloud products, Dataset, ftp://ladsweb.nascom.nasa.gov/MAS_eMAS/, 2015b.

NASA: Cloud Physics Lidar (CPL) level-2 optical product, Dataset, http://cpl.gsfc.nasa.gov/, 2015c.

Platnick, S.: Vertical photon transport in cloud remote sensing problems. J. Geophys. Res., 105, 22919–22935, 2000.

Platnick, S., Li, J. Y., King, M. D., Gerber, H., and Hobbs, P. V.: A solar reflectance method for retrieving the optical thickness and droplet size of liquid water clouds over snow and ice surfaces, J. Geophys. Res., 106, 15185–15199, doi:10.1029/2000JD900441, 2001.

Platnick, S., King, M. D., Ackerman, S. A., Menzel, W. P., Baum, B. A., Riédi, J. C., and Frey, R. A.: The MODIS cloud products: Algorithms and examples from Terra, IEEE T. Geosci. Remote., 41, 459–473, doi:10.1109/TGRS.2002.808301, 2003.

Platnick, S., King, M. D., Meyer, K. G., Wind, G., Amarasinghe, N., Marchant, B., Arnold, G. T., Zhang, Z., Hubanks, P. A., Ridgway, B., and Riedi, J.: MODIS cloud optical properties: User Guide for the Collection 6 Level-2 MOD06/MYD06 product and associated Level-3 datasets, available at: http://modis-atmos.gsfc.nasa.gov/_docs/C6MOD06OPUserGuide.pdf, 2015.

Rodgers, C. D.: Retrieval of atmospheric temperature and composition from remote measurements of thermal radiation, Rev. Geophys. Space GE, 14, 609–624, 1976.

Stamnes, K., Tsay, S.-C., Wiscombe, W., and Jayaweera, K.: A numerically stable algorithm for discrete-ordinate-method radiative transfer in multiple scattering and emitting layered media, Appl. Optics, 27, 2502–2509, 1988.

van Diedenhoven, B., Fridlind, A. M., Cairns, B., and Ackerman, A. S.: Variation of ice crystal size, shape, and asymmetry parameter in tops of tropical deep convective clouds, J. Geophys. Res., 119, 11809–11825, doi:10.1002/2014JD022385, 2014.

Veglio, P. and Holz, R.: Assessment of the sensitivity of a hyperspectral infrared cloud property retrieval to atmospheric parameters using an optimal estimation framework, Fall Meeting 2014, American Geophysical Union, San Francisco, California, 15–19 December 2014, A21C-3035, 2015.

Wang, C., Platnick, S., Zhang, Z., Meyer, K., and Yang, P.: Retrieval of ice cloud properties using an optimal estimation algorithm and the MODIS infrared observations. Part I: Forward model, error analysis, and information content, J. Geophys. Res., accepted, 2016a.

Wang, C., Platnick, S., Zhang, Z., Meyer, K., Wind, G., and Yang, P.: Retrieval of ice cloud properties using an optimal estimation algorithm and the MODIS infrared observations. Part II: Retrieval evaluation, J. Geophys. Res., in press, 2016b.

Yang, P., Liou, K. N., Wyser, K., and Mitchell, D.: Parameterization of the scattering and absorption properties of individual ice crystals, J. Geophys. Res., 105, 4699–4718, doi:10.1029/1999JD900755, 2000.

Yang, P., Bi, L., Baum, B. A., Liou, K. N., Kattawar, G. W., Mishchenko, M. I., and Cole, B.: Spectrally consistent scattering, absorption, and polarization properties of atmospheric ice crystals at wavelengths from 0.2 to 100 μm, J. Atmos. Sci., 70, 330–347, doi:10.1175/JAS-D-12-039.1, 2013.

Yorks, J. E., McGill, M., Hlavka, D., and Hart, W.: Statistics of Cloud Optical Properties from Airborne Lidar Measurements, J. Atmos. Ocean. Tech., 28, 869–883, doi:10.1175/2011JTECHA1507.1, 2011.